Energy 166 (2019) 951–960

Contents lists available at ScienceDirect

Energy

journal homepage: www.elsevier.com/locate/energy

Unlocking the coupling mechanical-electrochemical behavior of lithium-ion battery upon dynamic mechanical loading

Yikai Jia [a, b, 1], Sha Yin [a, b, 1], Binghe Liu [a, b], Hui Zhao [c, d], Huili Yu [c, d], Jie Li [c, d], Jun Xu [e, f, *]

[a] Department of Automotive Engineering, School of Transportation Science and Engineering, Beihang University, Beijing, 100191, China
[b] Advanced Vehicle Research Center (AVRC), Beihang University, Beijing, 100191, China
[c] Chongqing Changan Automobile Co. Ltd., Chongqing, 400023, China
[d] State Key Laboratory of Vehicle NVH and Safety Technology, Chongqing, 401120, China
[e] Department of Mechanical Engineering and Engineering Science, The University of North Carolina at Charlotte, Charlotte, NC 28223, United States
[f] North Carolina Motorsports and Automotive Research Center, The University of North Carolina at Charlotte, Charlotte, NC 28223, United States

ARTICLE INFO

Article history:
Received 7 July 2018
Received in revised form
20 October 2018
Accepted 24 October 2018
Available online 25 October 2018

Keywords:
Lithium-ion batteries
Safety
Dynamic loading
State-of-charge
Mechanical integrity

ABSTRACT

Dynamic mechanical loading, e.g. impact, is one of the major catastrophic factors that trigger short-circuit, thermal runaway, or even fire/explosion consequences of lithium-ion batteries (LIBs). In this study, the mechanical integrity and electrical coupling behaviors of lithium-ion pouch cells under dynamical loading were investigated. Two types of experiments, namely compression and drop-weight tests, are designed and conducted. The state-of-charge (SOC) and loading rate dependencies of batteries, as well as their coupling effect, are examined. Furthermore, the interaction between force response and electrical behavior of battery is investigated through real-time monitoring of voltage change during loading. Experiments on $LiCoO_2$ lithium-ion pouch cells show that the higher SOC and loading rates increases battery structure stiffness. In addition, loading rate intensifies battery structure stiffening with the SOC effect. Results indicate that the deformation and material failure of battery component together determine the electrical behavior of battery. Higher loading rate leads to faster voltage drop and more severe internal short-circuit. This short-circuit discharging process in turn affects the force response in dynamic loading. Results may provide useful insights into the fundamental understanding of electrical and mechanical coupled integrity of LIBs and lay a solid basis for their crash safety design.

1. Introduction

Lithium-ion battery (LIB) has become a universal power source for a variety of applications, including cell phones [1], laptops [2], and electric vehicles [3–7] due to its high energy/power density and extended cycle life [8,9]. However, the increasing number of fire/explosion incidents have caused extensive concerns on the safety aspects of LIB [10,11]. The complex nature caused by the coupling effects of mechanics and electrochemistry for batteries upon mechanical abusive loading calls for joint efforts from researchers, scientists and engineers from electrochemistry, mechanics, physics and material science. Therefore, the mechanical integrity of LIB has become a major research topic.

To directly investigate the electrochemical failure of LIB induced by mechanical abusive loading, experiments were designed and conducted to characterize the mechanical properties of battery cell in terms of structure [12] and its components [13,14] in quasi-static and dynamic loading conditions, where basic loadings include tension, compression [12,15,16], bending [12,17], indentation [12,17], penetration [18], and drop-weight [19].

From a multi-physical perspective, the mechanical behaviors of batteries are coupled with electrical performance. In a number of well-designed experiments [16,20], occurrence of voltage drop phenomenon was observed due to battery failure. Furthermore, the quantitative onset of short-circuit criteria was established based on the mechanical behaviors of LIBs, providing a novel method to evaluate the mechanical integrity of batteries [21]. In addition, Xu et al. discovered the strong relationship between mechanical structural stiffness and SOC in 18650 cylindrical battery cells [22]. Chen et al. discussed the strain rate and SOC effects on the

* Corresponding author. Department of Mechanical Engineering and Engineering Science, The University of North Carolina at Charlotte, Charlotte, NC 28223, United States.
E-mail address: jun.xu@uncc.edu (J. Xu).
[1] These authors contributed equally.

https://doi.org/10.1016/j.energy.2018.10.142
0360-5442/

mechanical and electric behaviors of lithium-ion cells [23]. Moreover, Arnold et al. studied the effect of mechanical stress on the electrical performance of LIBs and proposed a novel method for stage-of-health/SOC estimation by using simple mechanical measurements [24]. Recently, Wierzbicki et al. conducted series of dynamic intrusion tests on pouch cells and detected significant changes in critical force over a range of loading speed [25]. These research efforts explain a few of the mechanisms of the relationship between mechanical and electrical behaviors in relation to mechanical integrity.

In real-world engineering scenarios, the most catastrophic effect of mechanical abusive loading is the impact/crushing of LIBs. However, only a few studies are available to investigate the mechanical integrity and electrical behavior in the context of dynamic mechanical effect. In this case, the crash safety design of LIBs in electric vehicles have yet to be resolved. Hence, mechanical abusive tests in different loading rates and SOCs were designed to study the interaction between loading state and electrochemical behavior in this paper.

This paper is organized as follows. Section 2 describes the experimental methods, including sample preparation, experiment design, equipment, and data processing. Section 3 presents the typical results for quasi-static and dynamic mechanical experiments. Finally, Section 4 discusses and reveals the modes and mechanism of interaction effect between the electrical processes and mechanical behaviors.

2. Experimental

2.1. Sample preparation

A type of widely commercialized $LiCoO_2$ lithium-ion pouch battery was selected as the target cell as presented in Fig. 1 (a). The height, width, and depth of the battery are 6, 34, and 56 mm, respectively. The other specifications of the battery are listed in Table 1. The cell mainly consists of a jellyroll and an aluminum film. The laminated jellyroll consists of 48 layers of separators and 24 layers of cathodes and anodes.

The BK6808AR rechargeable battery performance testing device with a control computer was used to prepare battery samples. The charge and discharge cutoff voltages are summarized in Table 1, and the corresponding charge/discharge curve is shown in Fig. 1 (b). The cell was charged with a constant current to the designated SOC value, i.e., 0.2, 0.4, and 0.6 at 1 C rate.

2.2. Experiment method

Two groups of experiments were designed in this study, namely large-deformation compression tests and drop-weight experiments, to cover different loading rates from quasi-static to dynamic conditions. The displacements, loads, and voltages of the batteries were recorded in real time in a synchronized manner.

The INSTRON 8801 universal material testing machine with a compression test platform, which has a diameter of 110 mm, was used for the compression tests (Fig. 2 (a)). This machine has a

Table 1
Specifications of lithium-ion pouch battery test samples.

LIB parameters	Values
Charge cutoff voltage/V	4.2
Discharge cutoff voltage/V	2.7
Cathode/Anode materials	$LiCoO_2$/graphite
Nominal voltage/V	3.7
Nominal capacity/mAh	1250
Max charge/discharge current/C	10/10

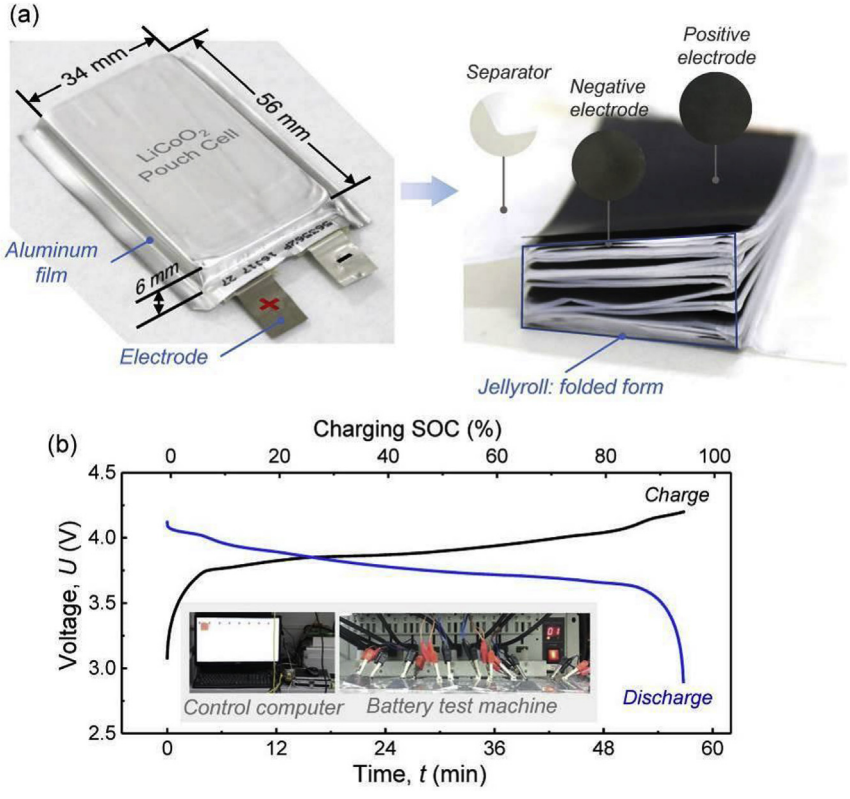

Fig. 1. (a) Geometry and components of selected $LiCoO_2$ lithium-ion pouch cell, (b) charge/discharge curve at 1 C for one experimental sample.

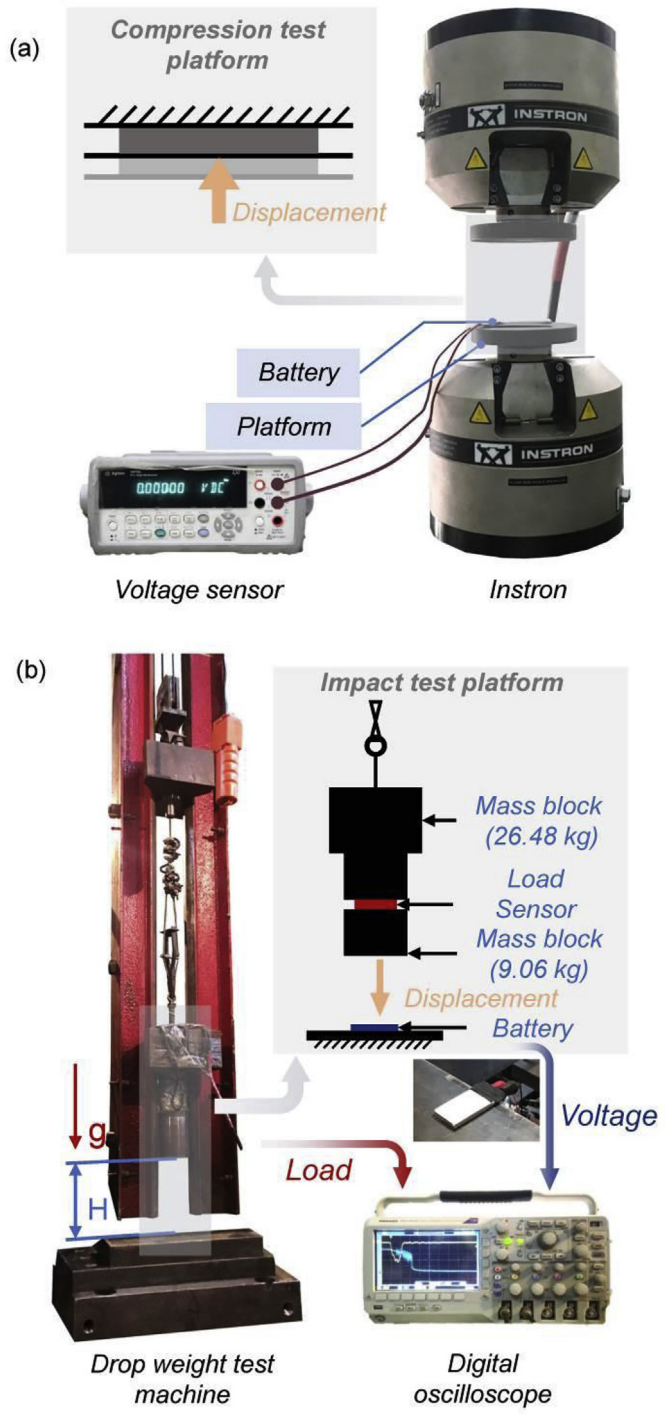

Fig. 2. Schematic illustration of (**a**) the compression experiment setup (the experimental equipment involves a universal material testing machine, a compression test platform and a voltage sensor) and (**b**) the drop-weight experiment setup (the experimental equipment involves a group of mass block, a load sensor, a digital oscilloscope and a test platform).

maximum load of 100 kN and an enhanced resolution of 50 N. Test accuracy was delimited to the maximum ±5% of the set value and 0.005% capacity of the load cell. The LIB voltage was measured *in situ* by the Agilent 34410A digital voltmeter with a recording frequency of 20 Hz and an accuracy of 0.01 mV. As shown in Fig. 2 (a), the battery was placed on the compression test platform, and two electrodes were connected to the digital voltmeter. When the experiment was carried out, the platform moved up and compressed the battery.

In the drop-weight experiment, the impact velocity and energy were determined based on the initial dropping height of the drop hammer. During loading, the displacement, load, and voltage of the batteries were simultaneously recorded in real time.

A drop-weight equipment comprising a mass block and a load sensor with a total weight of 35.54 kg was used for the drop tests (Fig. 2 (b)). The impact energy E was varied by changing the drop height while maintaining the drop-weights constant (Table 2). In this case, various drop height mimics various loading rate. In drop-weight experiment, the voltage and force (signal of the load sensor) were measured *in situ* by a digital oscilloscope at a recording frequency of 50 MHz and an accuracy of 0.01 V. As shown in Fig. 2 (b), the battery was placed on the drop-weight test platform, and two electrodes were connected to the digital oscilloscope. The mass block and load sensor were released when the experiment was carried out. The mass block with load sensor fell freely and thus crushed the battery.

After the load and mass values are determined, the loading speed, energy, and deformation displacement of the battery are calculated simply through Newton's law.

The initial velocity is calculated though the conservation of energy:

$$v_0 = \sqrt{2gH}, \tag{1}$$

where g is the gravitational acceleration, H is the initial height of mass block, which determines the impact energy:

$$E = mgH, \tag{2}$$

Table 2 provides the impact energy and the corresponding impact initial velocity that we selected in this paper. So, the impact energy and loading rate have one-to-one correspondence. The load was calculated through force analysis of mass block system (m_1-sensor-m_2):

$$F = kU_1\frac{m_1 + m_2}{m_2}, \tag{3}$$

where F is the force, U_1 is the signal of load sensor, k is conversion factor. The acceleration of the system a satisfies the following equation:

$$F - m_1 g = m_1 a, \tag{4}$$

Velocity v equals to the integral of acceleration:

$$v = v_0 + \int_0^t \left(\frac{F}{m_1} - g\right) dt, \tag{5}$$

Displacement d equals to the integral of velocity:

Table 2
Selected impact energy and loading rate from the drop-weight tests with various drop heights.

No.	1	2	3	4	5
Drop height (mm)	115	229	345	459	574
Impact energy (J)	40	80	120	160	200
Impact speed (m/s)	1.5	2.12	2.6	3	3.35

$$d = \int_0^t v \, dt, \tag{6}$$

3. Results

3.1. Compression test

We performed four test repetitions for compression experiment. The experiments had excellent repeatability from the perspective of load-displacement curve, the size and trend of load curves, as shown in Fig. 3 (a). Then, cases at 0.5 mm/min and 40 mm/min loading rates are selected as the typical results for the compression tests. Fig. 3 (b) clearly shows that load F slowly increases first but the growth rate of F gradually increases. The voltage in Fig. 3 (b) slightly increased from 3.756 V to 3.758 V during loading. The fundamental electrochemical mechanism of the slight voltage increase is probably due to the intercalation of a small amount of Li^+ in the graphite [22]. Obviously, this intercalation process is so tiny that its effect could be ignored. Experiments showed that short-circuit occurred when voltage started decreasing [21]. However, the internal short-circuit in this experiment was not triggered when F was within the range of the test machine (0–100 kN). As shown in Fig. 3 (c), when loading rate increases to 40 mm/min, load F rapidly and nearly linearly increases. By contrast, the voltage decreases from 3.756 V to 3.749 V with a corresponding gradient of −7.1 mV/mm after a short plateau stage (the dU/ds curve is shown in Fig. 3 (c)). The separator with saturated electrolyte should be regarded as liquid-solid mixture in dynamic loading considering the inertia of liquid flow. During this loading, the inertia effect of electrolyte lead to the unevenness of stress distribution over the sample. In this situation, the electrolyte tends to be extruded during deformation process but the electrolyte in center of battery is more difficult to be extruded from separator rather than electrolyte within the vicinity of brink. Excessive pressure compresses the separator in the central local area and makes the separator thin enough, leading to the small contact resistance between anode and cathode (current collector with electrode material coating) [26]. The internal short-circuit was triggered simultaneously (i.e. soft short-circuit [25], a kind of recoverable micro short-circuit). Moreover, the voltage starts to recover in the end of loading (after 1.6 mm displacement). After the unloading, the internal short-circuit is disconnected as the elastic deformation of separator recovered.

3.2. Drop-weight impact test

Take the case with initial loading speed of the mass block $v = 3$ m/s for example. As the loading proceeded, the speed gradually decreased to zero at $t = 0.8$ ms (i.e., 1.4 ms after the start of loading). The initial speed v is regarded as the nominal (impact) loading rate.

Fig. 3 (d) shows that load F rapidly increases and drops within 1.6 ms. The load– time curve (oscilloscope recording time) has some fluctuations nearby the peak value. This fluctuation is considered as the effect of electrical processes on dynamic mechanical behaviors. Radial deformation triggered the soft short-circuit. Then, heat produced by short-circuit current softened the components of battery, especially separator. After a soft process with force drop, the battery was compacted rapidly and force increased again. The increasing force continuously caused larger area of short-circuit introduced the force fluctuation until the electrochemical energy was drained.

The voltage decreased to ~2.5 V with a relatively low speed firstly. After that, the voltage sharply decreased to ~0.4 V (Fig. 3 (d)). Comparing with the abovementioned compression cases with a relatively low loading rate, the nonuniformity of cell deformation and stress distribution became more serious. Structural inertia effect caused by dynamic loading makes the short-circuit exhibited in the layer-by-layer and localized manner such that the short-circuit will be easily triggered in dynamic loading. Except for the squeezing of separator, the plastic deformation of current collector was also introduced. The folding of current collector leads to severe deformation of local area of separator. Therefore, the internal short-circuits (point A, soft short-circuit) were directly triggered by the loading. As the loading continues and deformation area extends, the internal micro short-circuits further evolves into the large area of short-circuit. The voltage falls to ~0.4 V rapidly (point B, hard short-circuits [25], a typical kind of unrecoverable short-circuit).

As shown in Fig. 3 (e), load F nearly linearly increases within the impact load process, thereby representing a linear elastic deformation before the first peak point. The voltage curve (Fig. 3 (e)) directly decreases with a gradient of −210 mV/mm during loading. Further, the dU/ds curve is shown in Fig. 3 (e) to reveal the relationship between force and voltage. Firstly, the dU/ds value increased from 0 mV/mm with the increasing of force in initial stage. This indicates that a larger force causes a faster decreasing rate of voltage. Then, the dU/ds started to fluctuate nearby 210 mV/mm with the force reached to its peak value. Finally, the dU/ds dropped in the unloading process. During the experiment, although the voltage did not recover to a stable value, the decreasing of the force did cause a transient slowing-down in the decreasing process of voltage.

4. Discussion

4.1. Loading rate dependent electrical-mechanical coupled behavior

There are two key factors dominating the mechanical behaviors of battery, i.e., SOC status and loading rate. First of all, the SOC-dependent mechanical behavior was studied through a group of LIBs with SOCs of 0.2, 0.4, and 0.6 via quasi-static compression experiment (where loading rate is 0.5 mm/min). Generally, the stiffness of high SOC batteries is larger than that of low SOC batteries, as shown in the three typical curves in Fig. 4 (a). Quantitatively similar results in 18650 $LiCoO_2$ LIBs were reported by a previous study [22]. Thus, different types of LIBs share similar SOC hardening behaviors. Such phenomenon can be attributed to the insertion of Li^+, which further enhances the initial stress of the graphite anode and stiffens the structure [27]. It is noteworthy that this SOC-hardening effect also existed in dynamic loading tests. We selected a group of LIBs with SOC = 0.2/0.4 for the drop-weight experiments to explore this effect of SOCs. The load values at the peak point (maximum value of force) were extracted from force-time curves. The peak load in SOC = 0.4 cases were relatively higher than them in SOC = 0.2 cases (Fig. 4 (b)). In addition, the peak load and the gradient of the peak load–energy curves increased with the increase in impact energy.

Apart from that, the loading rate is a more decisive factor. Fig. 4 (c) shows the load–displacement curves of LIBs at SOC = 0.2 with various loading rates (0.5 mm/min, 20 mm/min, 40 mm/min from the quasi-static compression tests and 2.6 m/s, 3.4 m/s from the drop-weight tests) to investigate the relationship between deformation and mechanical response. The batteries exhibit high structural stiffness with loading rate. This loading rate dependent "hardening effect" is more obvious than SOC-dependent hardening, indicating a much deteriorated safety scenario in real-

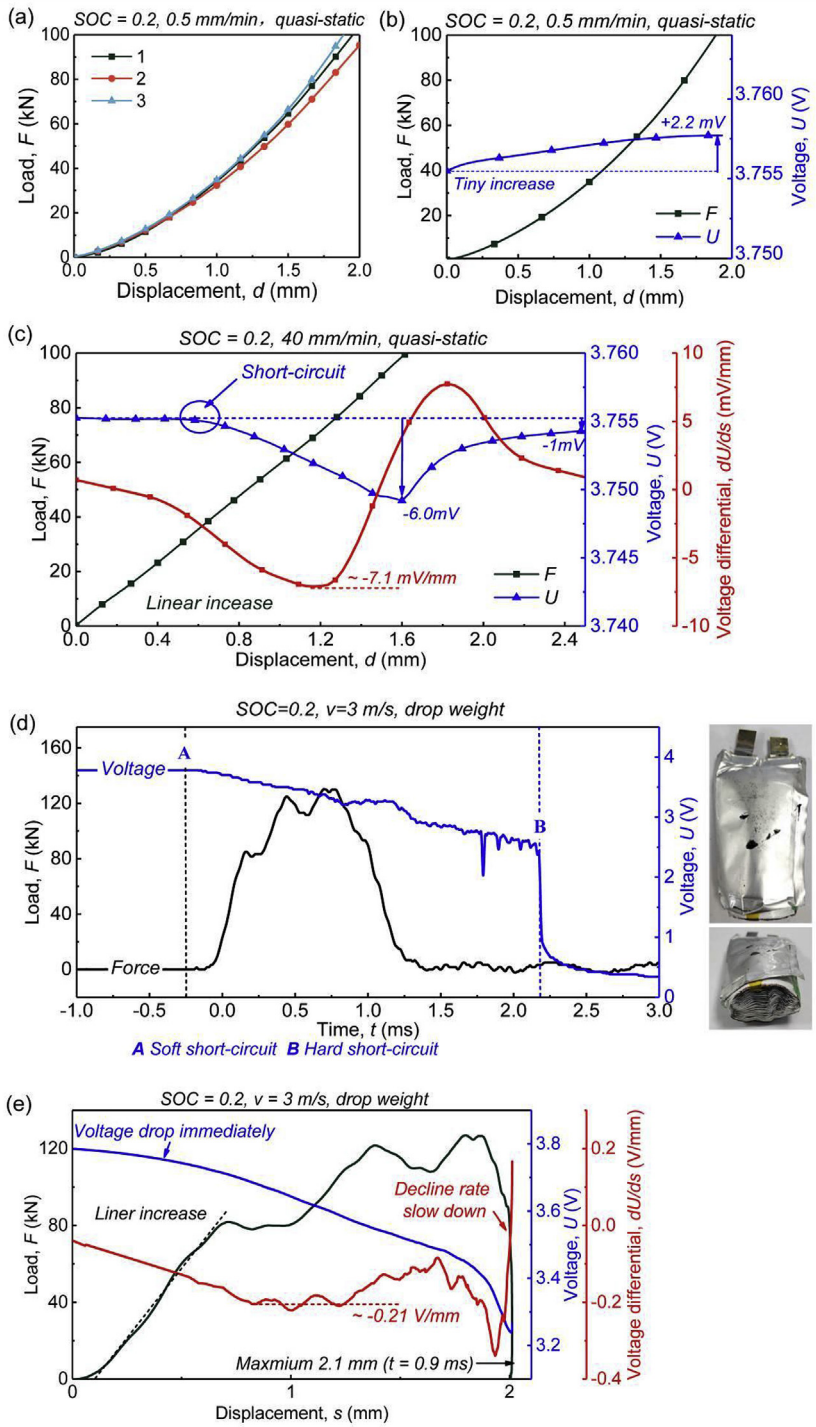

Fig. 3. (**a**) Load-displacement curves of three batteries with SOC = 0.2. Typical mechanical and electrical behaviors in compression loadings, which include force and voltage displacement during the compression test for the battery at SOC = 0.2 and various loading rates: (**b**) 0.5 mm/min and (**c**) 40 mm/min. Typical mechanical and electrical behaviors in dynamic impact load: (**d**) force–, voltage– and impact speed-time curves and (**e**) force– and voltage–displacement curves during drop-weight testing for battery at SOC = 0.2, where the loading rate is 3 m/s.

world dynamic impact accidents. Further, the estimated effective compressive elastic moduli were shown in Fig. 4 (d). The logarithm of *v* has liner relationship with initial tangent modulus. On one hand, the inertia effect of battery structural and the constitute component materials leads to large reaction forces measured by the sensor, which is a similar behavior observed in other structures [19]. On the other hand, strain rate -effect of electrode materials also plays an important role in dynamic loading, leading to a stiffened mechanical behavior of the cell. L. Wang et al. pointed out that effective module, yield stress and failure stress of the cylindrical battery cell increases with the increasing of strain rate [28]. Straightforwardly, a more dangerous situation is expected for high SOC batteries upon high loading rate.

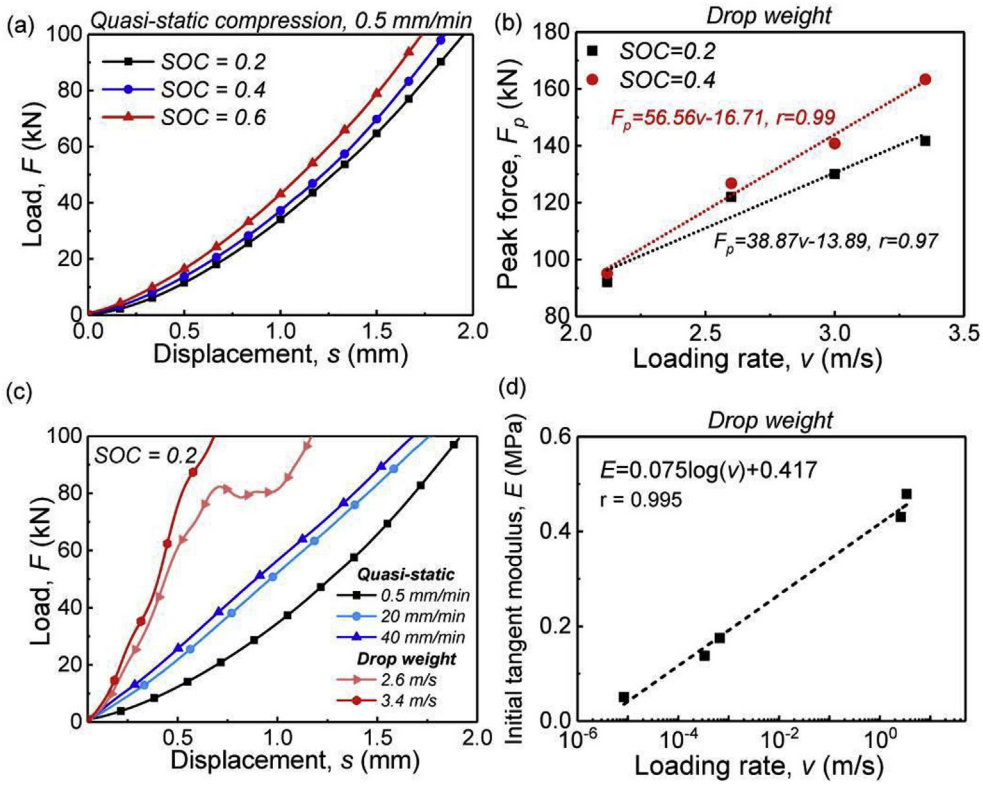

Fig. 4. (**a**) Load–displacement curves of LIBs at various SOC values with a loading rate of 0.5 mm/min. (**b**) Peak load–impact energy curves of LIBs at SOC = 0.2 and 0.4. (**c**) Load–displacement curves and (**d**) initial tangent modulus of LIBs at various loading rate (the loading rate in drop-weight was regarded as constant in preliminary stage (0–0.5 mm)) with SOC = 0.2.

4.2. Effect of loading rate on initial voltage drop rate

As a critical factor, loading rate not only affects the force response, but also the voltage drop behavior. Fig. 5 shows the voltage–displacement curves of LIBs at SOC = 0.2 with various loading rates for the quasi-static compression tests and various impact energy for the drop-weight tests. The gradient of the voltage change decreased with loading rate for the quasi-static compression test (Fig. 5 (a)). The slight voltage increases in the initial stage in all cases (i.e., 0.5 mm/min, 20 mm/min, 40 mm/min) can probably be attributed to the intercalation of a small amount of Li^+ in the graphite [22]. However, with the increase in loading rate, the voltage decreases in the next stage (20 mm/min and 40 mm/min). With the end of loading (the machine reached its range), the voltage stopped decreasing and started to recover (loading termination lines in Fig. 5 (a)).

As shown in Fig. 5 (b), the gradient of voltage drop for the drop-weight impact test is much larger than that in quasi-static case cases. The curves are in agreement due to the nearly similar magnitudes of their respective impact velocities (form 1.5 m/s to 3.35 m/s). It is the larger deformation rate leads to the quicker voltage drop because a large deformation rate causes a more localized stress distribution. Deformation of large area of separator and plastic deformation of current collectors lead to severe internal short-circuits.

The summary of experimental data in Table 3 shows that an increase in loading rate leads to the increase in voltage drop rate. Therefore, increasing the loading rate can easily cause battery failure from the perspective of mechanical integrity.

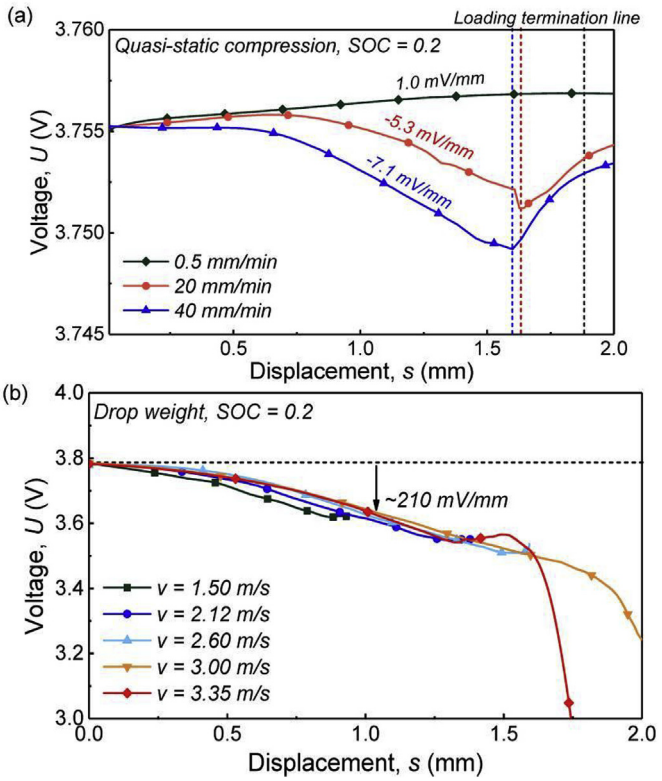

Fig. 5. Voltage–displacement curves of the battery at SOC = 0.2 in various loading rates: (**a**) compression tests and (**b**) drop-weight tests.

Table 3
Summary of the relationship between loading rate and voltage drop rate.

	1	2	3	4
Loading rate (m/s)	8.3×10^{-3} (0.5 mm/min)	3.3×10^{-1} (20 mm/min)	6.7×10^{-1} (40 mm/min)	3.4
Voltage drop rate (mV/mm)	+1	−5.3	−7.1	−258

4.3. Interaction between force response and electrical process

For dynamic impact experiments, force curves share a similar profile regardless of SOC and loading rate (Fig. 6). This phenomenon indicates that the force fluctuation is time-dependent (namely, the fluctuation triggers at a specific timing) rather than force-dependent or deformation-dependent. One step further, such force peaks should be highly related to the electrochemical behavior of the cell given the fact that internal short-circuit is triggered way before the first force peak. Take the case with SOC = 0.2 for example (Fig. 6(a)). The voltage drop becomes more obvious with force increase drastically. It indicates that a larger force would cause a more severe soft short-circuit status and a larger decreasing rate of voltage. When it reaches the second force peak, the voltage drop becomes extremely fast. In particular, in cases with $v = 3$ m/s and $v = 3.35$ m/s, transitions from soft short-circuit into hard short-circuit or open-circuit can be observed.

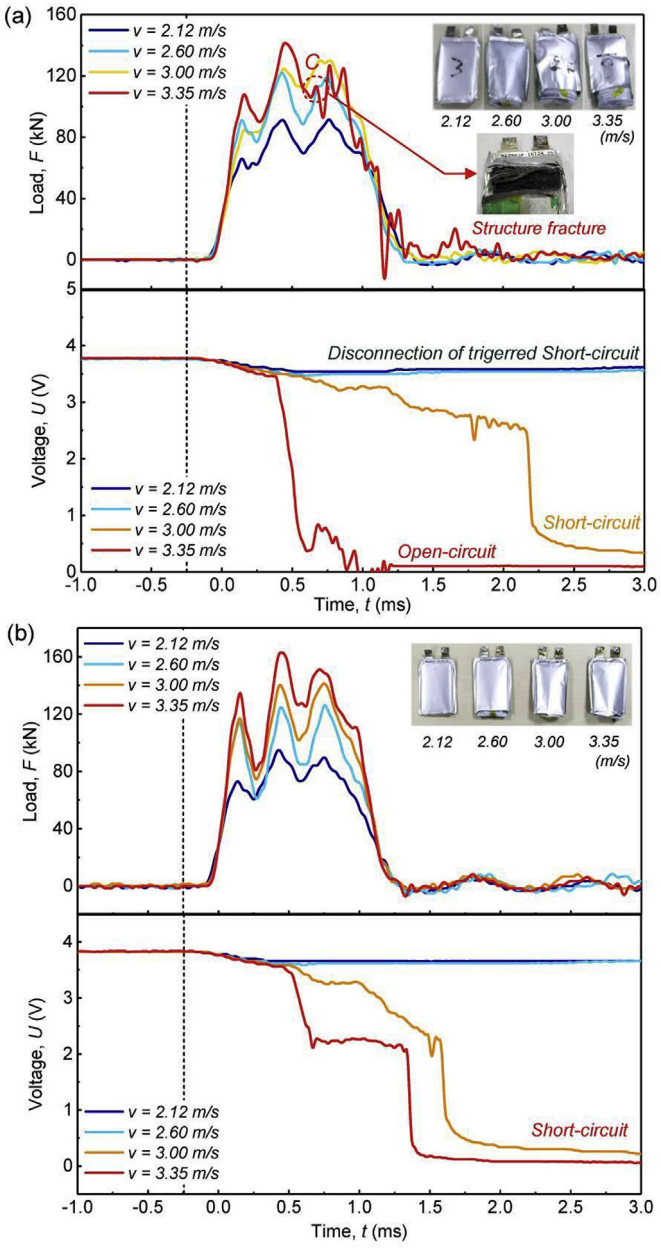

Fig. 6. Load - time curves and correspondingly voltage - time curves of LIBs at (**a**) SOC = 0.2 and (**b**) SOC = 0.4 for various loading rates.

As the statement above, the SOC of the batteries may cause a hardening effect in mechanical behaviors. Such effect further leads to a change of short-circuit behaviors of batteries. When SOC increases from 0.2 to 0.4, the decreasing rate of voltage tends to increase, especially in $v = 3.0$ m/s case (Fig. 6 (b)). This tendency could be explained as the hardening effect from SOC. As the

SOC increases, the battery becomes harder and the force response increases. Considering a larger force causes a larger decreasing rate of voltage, a larger SOC of battery also leads to a larger decreasing rate of voltage in dynamic impact loading.

4.4. Modes and mechanism of battery failure on dynamic loading

Three typical modes of battery failure on dynamic loading can be abstracted from the experimental data of the drop weigh tests of batteries at SOC = 0.2:

Mode 1: the batteries do not completely fail electrochemically. When v = 2.6 m/s, the batteries did not completely fail in electrochemical performance. Instead, soft short-circuit occurred, and the voltage curves slowly decreased with approximately 200 mV voltage drop (Fig. 7 (a)). After unloading, the voltage slightly recovered.

Mode 2: the batteries completely lose their capacity. The voltage curve can be divided into two stages. As shown in Fig. 7 (b), when v = 3 m/s, the voltage curves gradually decreased initially (Stage 1). Then, the voltage curves dropped to a relatively low value (~0.4 V) (Stage 2). Moreover, the force response followed the same pattern as v = 2.6 m/s case.

Mode 3: the batteries lose their capacity. However, the duration of Stage 1 is relatively short and the voltage curves immediately decrease to zero in Stage 2, such as the case of $v = 3.35$ m/s (Fig. 7 (c)). Furthermore, the voltage decrease behavior in the stage 2 of $v = 3$ m/s cases is a typical behavior of short-circuit battery, in which voltage approached to a low value rather than zero. While for $v = 3.35$ m/s cases, the voltage dropped to zero which is a behavior of open-circuit battery. This point could be demonstrated by the pictures in Fig. 6 (a) (Point C, structure failure of battery). Apart from that, the force response did not follow the similar pattern, as $v = 2.6$ m/s and $v = 3.0$ m/s cases, after the point C.

The voltage-drop mode changes with loading rate increases. A relatively faster loading speed can lead to severe damage due to high mechanical force and large battery deformation. However, all of the voltage curves demonstrated a relatively slow decreasing stage. In this stage, the internal micro short-circuits (soft short-circuit) is recoverable in case of loading termination.

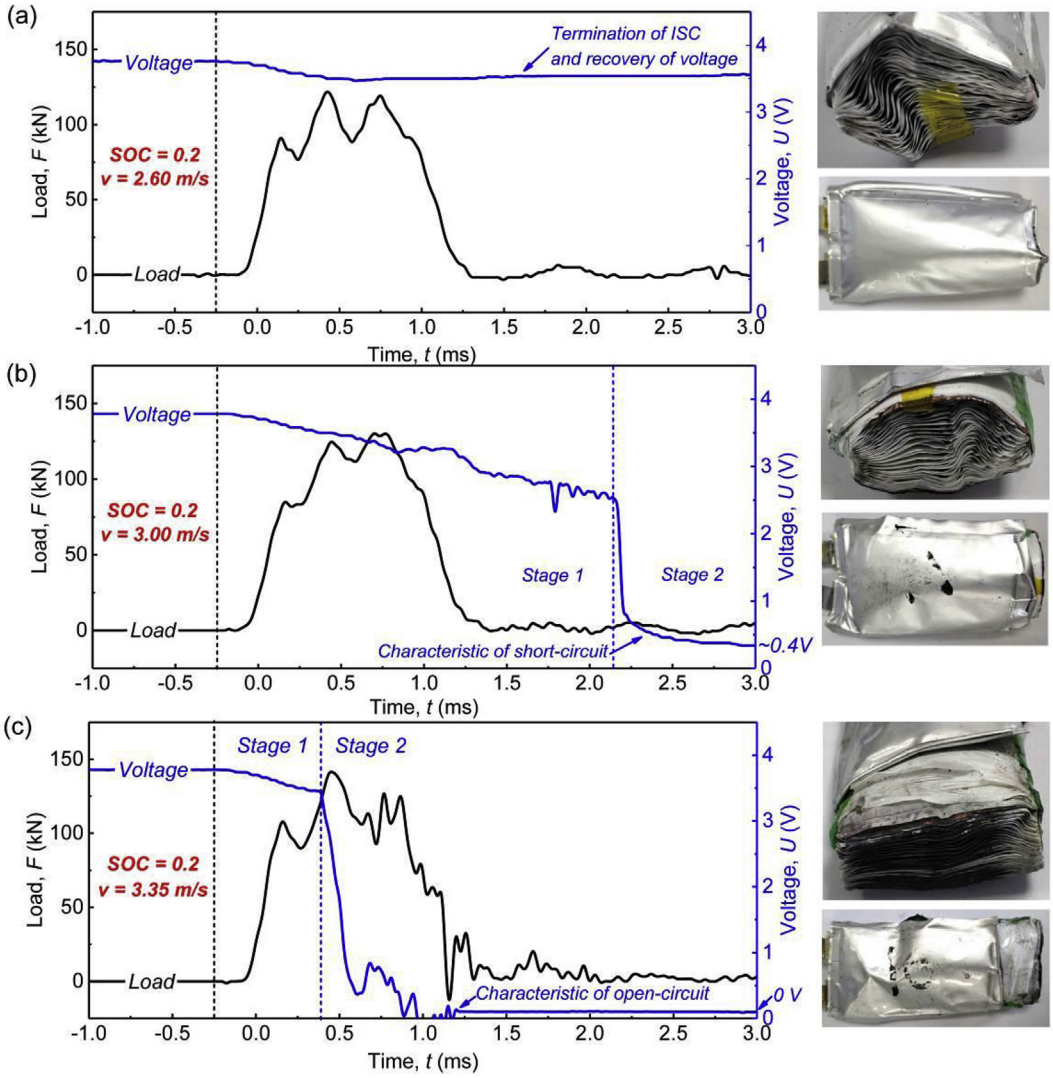

Fig. 7. Electrical failure behaviors of batteries at SOC = 0.2 in various impact energies during the drop-weight tests: (**a**) $v = 2.6$ m/s; (**c**) $v = 3$ m/s and (**e**) $v = 3.35$ m/s.

Furthermore, the pattern of the force curves changed with different electrochemical status of batteries. The force curves followed a same pattern in most short-circuit cases, while them would have some changes if the open short-circuit occur.

Through the deformation of battery components, the mechanism of those three modes were revealed. As the increasing of the impact energy, the deformation of the battery components became more severe (Fig. 8). Take the cathode for example, deformation model in 2.6 m/s case is radically different from 3 m/s case and 3.35 m/s. The folds of 2.6 m/s case mostly in one direction, length wise direction, while they tend to be omnidirectional in other cases. Apart from that, the degree of materials failure became more seriously as the loading rate increased. Some exposed electrode layers were observed in the positive electrode surface. A crack was found in cathode, anode and separator of 3 m/s case while complete breakage occurred in the same position in 3.35 m/s case. It is worth to note that separators have some folds and transparent area in all cases.

The deformation model determined the modes of short-circuit behaviors. In low impact energy case (Mode 1), the plastic deformation of current separator is regular and just a few short-circuit points. When loading rate increases (Mode 2), the plastic deformation tends to be irregular and more short-circuit points are involved. The large area of short-circuit exhausts the electrical energy of battery drastically. In the high impact energy case (Mode 3), the force is too large such as to tear the battery apart. The open-circuit will trigger immediately rather than draining off the battery power via short circuit.

5. Conclusion

In this study, we experimentally investigated the mechanical integrity of lithium-ion pouch cells under dynamic loadings. Compression under quasi-static loading and drop-weight impact tests were designed and conducted. By establishing a test matrix that considering various SOCs (SOC = 0.2/0.4) and loading rates ($v = 1.5$–3.35 m/s), the SOC- and loading rate-dependent as well as the coupling effect of these two factors were explored. Furthermore, through *in situ* and synchronized monitoring of voltages during loading, the relationship between electrical discharging process and force response of batteries was investigated. The experiments on $LiCoO_2$ lithium-ion pouch cells show that the increases in SOC and loading rate leads to battery structure stiffness. The maximum peak forces of the drop-weight impact tests increase with SOC and loading rate. High loading rate leads to considerable changes in peak force after increasing SOC.

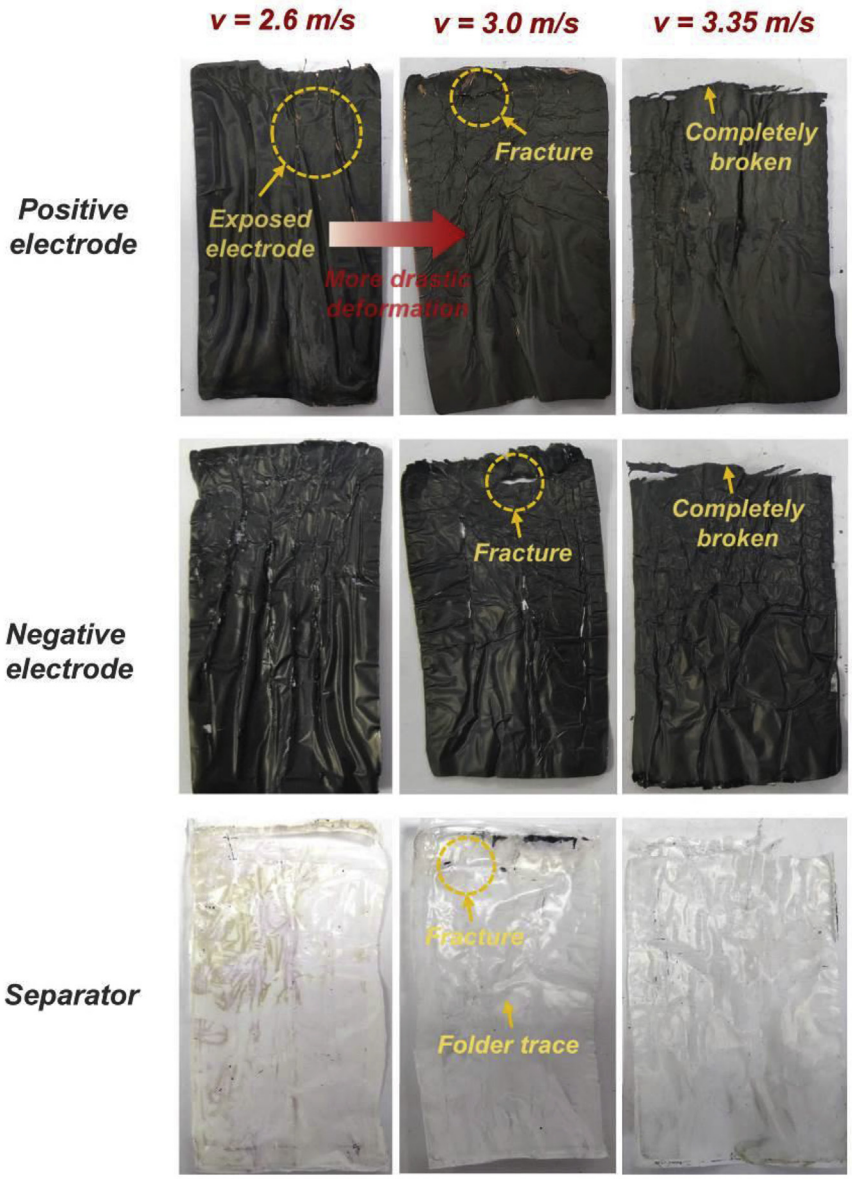

Fig. 8. Surface morphology of battery components (including cathode, anode and separator) upon various loading rate.

Moreover, three typical modes of battery failure on dynamic loading are abstracted:

- Mode 1: the batteries did not completely fail in electrochemical performance. The plastic deformation of current separator is regular and just a few short-circuit points.
- Mode 2: the batteries completely lost their capacity. The voltage curves gradually decreased initially (Stage 1). Then, the voltage curves dropped to a relatively low value (~0.4 V) (Stage 2). The plastic deformation tends to be irregular and more short-circuit points were involved. The large area of short-circuit exhausted the electrical energy of battery drastically.
- Mode 3: the batteries also lost their capacity. However, the duration of Stage 1 is relatively short and the voltage curves immediately decreased to zero in Stage 2. The force was too large such as to tear the battery apart. The open-circuit occurred immediately rather than short-circuit to drain off the battery power.

The component deformation and materials failure state of battery determine the electrochemical discharging (voltage drop) behavior during short-circuit process of battery. Higher loading rate, causes a faster voltage-drop and more severe internal short-circuit. This short-circuit discharging process in turn affects the force response in dynamic loading.

Results indicate remarkable differences of mechanical behavior, electrochemical behavior and failure mechanisms of LIBs in dynamic impact and provide useful insights for the mechanical integrity of LIBs and their crash-safety design.

Author contributions statement

J.X. and S.Y. designed the study. Y.K.J and B.H.L. set up and performed the experiments. H.Z., H.L.Y. and J.L. help with the pouch cell samples and data processing of mechanical tests. Y.K.J and J.X. drafted the manuscript, and J.X. and S.Y. revised the manuscript and contributed to discussions throughout the project.

Acknowledgement

This work is financially supported by The National Key Research and Development Program of China (2017YFB0103703), Opening project of State Key Laboratory of Explosion Science and Technology (KFJJ17-13M), Research Project of the State Key Laboratory of Vehicle NVH and Safety Technology (NVHSKL-201610).

Appendix A. Supplementary data

Supplementary data to this article can be found online at https://doi.org/10.1016/j.energy.2018.10.142.

References

[1] Armand M, Tarascon JM. Building better batteries. Nature 2008;451(7179):652–7.
[2] Scrosati B, Garche J. Lithium batteries: status, prospects and future. J Power Sources 2010;195(9):2419–30.
[3] Vikström H, Davidsson S, Höök M. Lithium availability and future production outlooks. Appl Energy 2013;110:252–66.
[4] Ovrum E, Bergh TF. Modelling lithium-ion battery hybrid ship crane operation. Appl Energy 2015;152:162–72.
[5] Densing M, Turton H, Bäuml G. Conditions for the successful deployment of electric vehicles – a global energy system perspective. Energy 2012;47(1):137–49.
[6] Hedegaard K, Ravn H, Juul N, Meibom P. Effects of electric vehicles on power systems in Northern Europe. Energy 2012;48(1):356–68.
[7] Shokrzadeh S, Bibeau E. Sustainable integration of intermittent renewable energy and electrified light-duty transportation through repurposing batteries of plug-in electric vehicles. Energy 2016;106:701–11.
[8] Ferreira HL, Garde R, Fulli G, Kling W, Lopes JP. Characterisation of electrical energy storage technologies. Energy 2013;53:288–98.
[9] Li Y, Wang C, Gong J. A combination Kalman filter approach for State of Charge estimation of lithium-ion battery considering model uncertainty. Energy 2016;109:933–46.
[10] Bandhauer TM, Garimella S, Fuller TF. A critical review of thermal issues in lithium-ion batteries. J Electrochem Soc 2011;158(3):R1–25.
[11] Kvasha A, Gutiérrez C, Osa U, de Meatza I, Blazquez JA, Macicior H, et al. A comparative study of thermal runaway of commercial lithium ion cells. Energy 2018;159:547–57.
[12] Sahraei E, Hill R, Wierzbicki T. Calibration and finite element simulation of pouch lithium-ion batteries for mechanical integrity. J Power Sources 2012;201:307–21.
[13] Lai W-J, Ali MY, Pan J. Mechanical behavior of representative volume elements of lithium-ion battery cells under compressive loading conditions. J Power Sources 2014;245:609–23.
[14] Cannarella J, Liu X, Leng CZ, Sinko PD, Gor GY, Arnold CB. Mechanical properties of a battery separator under compression and tension. J Electrochem Soc 2014;161(11):F3117–22.
[15] Xu J, Jia Y, Liu B, Zhao H, Yu H, Li J, et al. Coupling effect of state-of-health and state-of-charge on the mechanical integrity of lithium-ion batteries. Exp Mech 2018;58(4):633–43.
[16] Liu B, Zhao H, Yu H, Li J, Xu J. Multiphysics computational framework for cylindrical lithium-ion batteries under mechanical abusive loading. Electrochim Acta 2017;256:172–84.
[17] Sahraei E, Kahn M, Meier J, Wierzbicki T. Modelling of cracks developed in lithium-ion cells under mechanical loading. RSC Adv 2015;5(98):80369–80.
[18] Feng X, Lu L, Ouyang M, Li J, He X. A 3D thermal runaway propagation model for a large format lithium ion battery module. Energy 2016;115:194–208.
[19] Xu J, Liu BH, Wang LB, Shang S. Dynamic mechanical integrity of cylindrical lithium-ion battery cell upon crushing. Eng Fail Anal 2015;53:97–110.
[20] Wierzbicki T, Sahraei E. Homogenized mechanical properties for the jellyroll of cylindrical Lithium-ion cells. J Power Sources 2013;241:467–76.
[21] Greve L, Fehrenbach C. Mechanical testing and macro-mechanical finite element simulation of the deformation, fracture, and short circuit initiation of cylindrical Lithium ion battery cells. J Power Sources 2012;214:377–85.
[22] Xu J, Liu BH, Hu DY. State of charge dependent mechanical integrity behavior of 18650 lithium-ion batteries. Sci Rep 2016;6:21829.
[23] Tsutsui W, Siegmund T, Parab ND, Liao H, Nguyen TN, Chen W. State-of-Charge and deformation-rate dependent mechanical behavior of electrochemical cells. Exp Mech 2017:1–6.
[24] Cannarella J, Arnold CB. State of health and charge measurements in lithium-ion batteries using mechanical stress. J Power Sources 2014;269:7–14.
[25] Kisters T, Sahraei E, Wierzbicki T. Dynamic impact tests on lithium-ion cells. Int J Impact Eng 2017;108:205–16.
[26] Liu B, Jia Y, Li J, Yin S, Yuan C, Hu Z, et al. Unlocking safety issues caused by internal short circuits in lithium-ion batteries. J Mater Chem 2018. https://doi.org/10.1039/C8TA08997C.
[27] Fu R, Xiao M, Choe S-Y. Modeling, validation and analysis of mechanical stress generation and dimension changes of a pouch type high power Li-ion battery. J Power Sources 2013;224:211–24.
[28] Wang L, Yin S, Zhang C, Huan Y, Xu J. Mechanical characterization and modeling for anodes and cathodes in lithium-ion batteries. J Power Sources 2018;392:265–73.